

## INFLUENCE OF THE WELDING SPEED ON FSW JOINTS ON 7049A ALUMINIUM ALLOY

### Uticaj brzine zavarivanja na FSW spojeva na leguri aluminijuma 7049A

Tomaž Vuherer<sup>1</sup>, Milenko Perović<sup>2</sup>, Darko Bajić<sup>3</sup>, Sebastian Baloš<sup>4</sup>

<sup>1</sup> University of Maribor, Faculty of Mechanical Engineering, Maribor, Slovenia

<sup>2</sup> Chamber of Economy of Montenegro, Podgorica, Montenegro

<sup>3</sup> University of Montenegro, Faculty of Mechanical Engineering, Podgorica, Montenegro

<sup>4</sup> University of Novi Sad, Faculty of Technical Science, Serbia

**Ključne riječi:** FSW, zatezna čvrstoća, lomna žilavost, tvrdoća, udarna žilavost

#### Sažetak

U radu je analiziran utjecaj brzine zavarivanja na mehanička svojstva dva spoja zavarena trenjem miješanjem (FSW). Kao osnovni material, za ispitivanje je korišćena homogenizirana i umjetno starena višekomponentna Al-Zn-Mg-Cu legura. Ispitivanje istezanjem, mjerenje tvrdoće, instrumentirano Charpy ispitivanje, SENB ispitivanje mehanizma loma i analiza mikrostrukture izvršena je na dva uzorka koji su zavareni različitim brzinama zavarivanja. Istraživanja su pokazala da spojevi zavareni većom brzinom zavarivanja imaju bolja mehanička svojstva i prikladniju mikrostrukturu.

**Keywords:** FSW, tensile strength, fracture toughness, hardness, impact toughness

#### Abstract

Influence of welding speed on mechanical properties of two weld joints welded by Friction Stir Welding (FSW) were studied in this paper. In this research homogenized and artificially aged multicomponent Al-Zn-Mg-Cu alloy was used as a base material. Tensile tests, hardness measurements, instrumented impact Charpy tests, fracture mechanics SENB tests and microstructure analysis were done on two different weld joints welded by different welding speed. The study revealed that weld joint welded by higher welding speed have better properties and more convenient microstructure.

### 1. Introduction

Welding of heat treated and aged aluminium alloys was in some cases an insurmountable problem for conventional welding processes. Especially big challenge represented welding of aluminium alloys EN AW 7xxx series, which forms system Al-Zn-Mg-Cu (4,3% to 7,7% Zn), due to sublimation of the zinc during welding.

FSW (Friction Stir Welding) presents one of the alternatives how to overcome previously mentioned problems during welding [1-3]. Commonly, these alloys are used for aerospace industry and rocket building technology, therefore from the base material and weld joints are expected to ensure high strength, appropriate hardness, high impact and fracture toughness as well as increased sensitivity to the cracks.

Schematically the FSW process is shown in Figure 1 [4]. Some parts of which FSW weld joints are constituted are usually non-symmetric shape (weld nugget, thermomechanical affected zone - TMAZ, and head affected zone - HAZ), due asymmetry which occurs at welding on the advancing and retreating side of the pin.

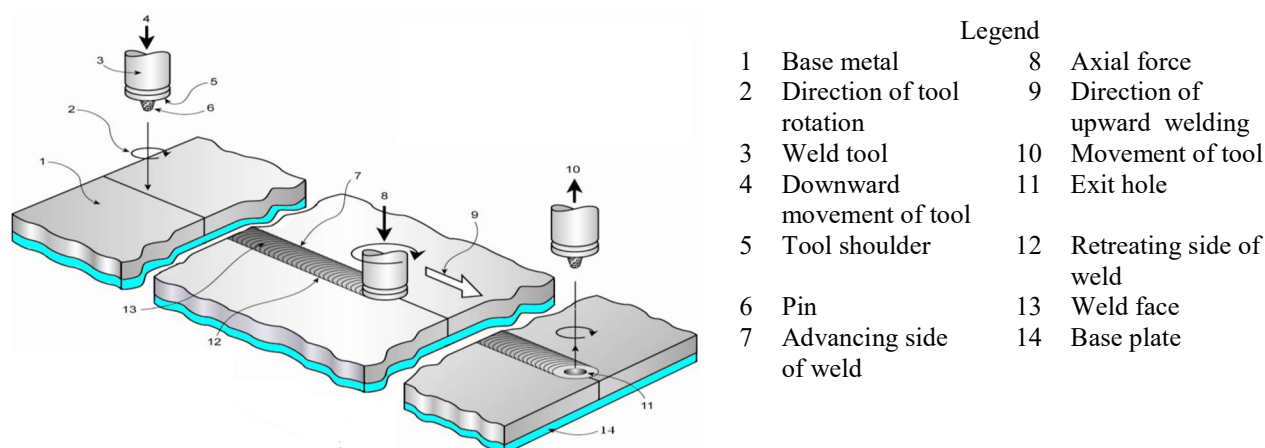


Fig. 1 Scheme of the friction stir welding process [3]

## 2. Material

Aluminium alloy 7049A alloy (Al-Zn-Mg-Cu in condition T652) is used as a base material in this investigation. Thanks to its physical and mechanical characteristics, this alloy has a very convenient ratio of the mass and strength, so normally it is used for aerospace industry and rocket ship building. High strength appropriate hardness, high impact and fracture toughness are expected from the alloy.

Chemical analysis was carried out by Pechiney's OE quant-meter ARL 3580 [5,6]. Chemical composition of the base material is shown in Table 1 and its mechanical properties are represented in Table 2.

Table 1 Chemical composition of the base material

Content of elements, weight %										
Zn	Mg	Cu	Mn	Cr	Zr	Ti	V	B	Fe	Si
7.28	2.25	1.58	0.29	0.18	0.14	0.15	0.007	0.003	0.16	0.09

Table 2 Mechanical properties of the base material

$R_{p0.2}$ (MPa)	$R_m$ (MPa)	$A_5$ (%)	Hardness (HB)
506	588	8	160

## 3. Experimental procedure

**Welding:** Two different weld joint were welded by FSW process. Weld joints were welded on the two plates with dimension of  $180 \times 65 \times 6$  mm. The shape and geometry of the tool and pin are shown in Figure 3. The tool was made from high-alloyed tool steel, which was finally heat treated to achieve hardness of the 54 HRC.

Welding is carried out by CNC milling machine AG 400 by continuous supervising of the tool revolution speed and welding speed (table traveling). Figure 4 shows experimental workplace during welding, where heat flow was measured.

Welding parameters are represented in Table 3. Two different welding speeds were used for welding. Other parameters of welding are remained equal during both weldings.

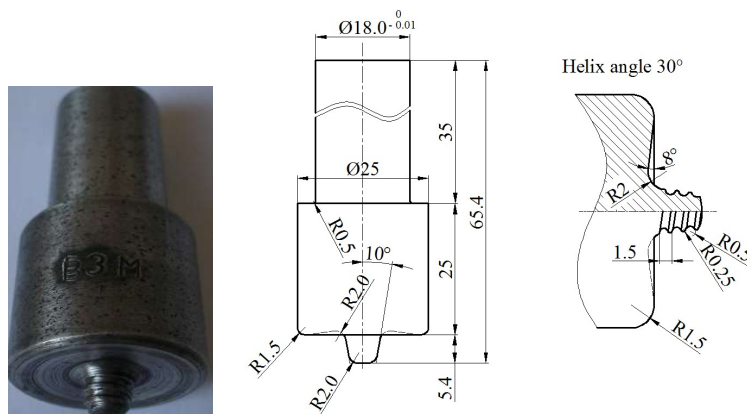


Fig. 3 Shape and geometry of the FSW tool



Fig. 4. Experimental workplace

Table 3 Welding parameters

Weld Joint	Tool revolutions speed ( $\text{min}^{-1}$ )	Welding speed ( $\text{mm}/\text{min}$ )	Tool angle (backward) ( $^{\circ}$ )	Speed of tool penetration ( $\text{mm}/\text{s}$ )	Penetration depth (mm)
A	750	60	1	0.01	5.4 + 0.2
B	750	80	1	0.01	5.4 + 0.2

**NDT inspections;** All weld joints were inspected by different NDT inspection methods [7,8]. VT (visual testing), PT (penetrant testing) and RT (radiography testing by x-rays) were used for the inspection. The results of the PT inspection are shown in Figure 5, where some mistakes were appeared at the end of weld joint. These mistakes are present in both joints located at the position where the pin for the welding was pulled out of the weld. This part of the joint is not usable because a hole remained in the weld joint as a consequence of pin removing. Other parts of both welded joints were without defects.



Fig. 5 NDT inspection of weld joints by liquid penetrant

Results of RT inspection are presented in Figure 6. Both welds are without defects, with the exception of the end of weld joints, which is considered to be a normal result of FSW process due to pin removing.

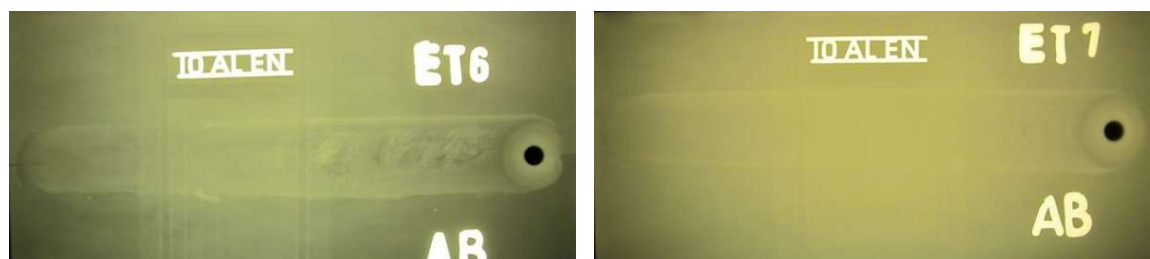


Fig. 6 NDT inspection of weld joints by X-ray radiography

Different methods and techniques for the determination of the individual weld joint properties were used for characterisation of weld joint properties, such as:

- tensile test,
- hardness measurements,
- Charpy impact test,
- fracture mechanics,
- microstructure analysis.

Table 4 shows used experimental tests and techniques at the investigation and location where the specimen were cut from and machined out. The numbers of the specimens for each test for the both types of the weld joints are also presented in this table.

Table 4 Plan of specimens

Type of specimens	Type of weld joint	
	A	B
Tensile specimens (weld joint, base material)	1	1
Charpy specimens (weld nugget, TMAZ, HAZ, BM)	7	7
Macro section for hardness measurement (weld joint)	1	1
Micro section for microstructure analysis (weld joint)	1	1
SENB specimens (weld nugget, BM)	2	2

**Tensile tests:** Geometry of the tensile specimens, which were machined from weld joint and base material, and shape of the specimens from weld joint are exposed in Figure 7. Tensile tests were carried out according to standard EN ISO 6892-1.

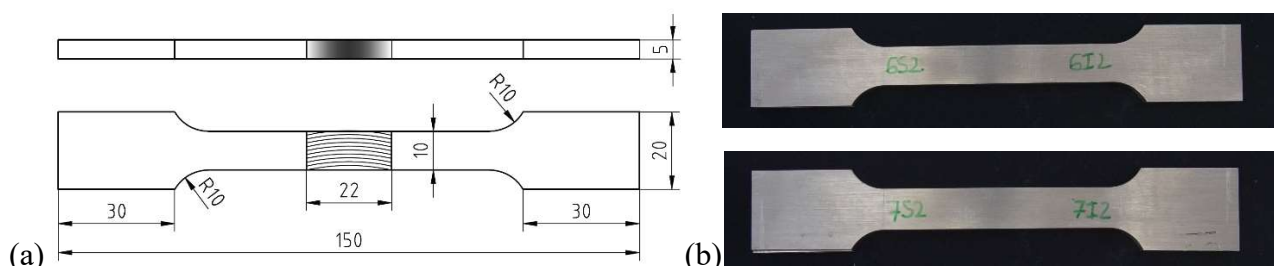


Fig. 7 Geometry of the tensile specimen and shape of the tensile specimens

**Instrumented Charpy impact tests:** Geometry and shape of the reduced Charpy specimen are presented in Figure 8. The standardised 2 mm deep ISO-V notch with radius of 0.25 mm was used as a stress concentrator during the Charpy impact tests. Instrumented impact tests were performed according to EN ISO 148-1 and ASTM E2290-15. Energy for fracture was divided into the energy for initiation and into the energy for propagation of the crack from ISO-V-notch stress concentrator.

Force versus time diagrams were recorded during the tests. The Charpy specimens with ISO-V notch located on different regions were used in this investigation such as:

- weld nugget (weld centre),
- TMAZ (4 mm from the weld centre at the advancing and the retreating side of the weld),
- HAZ (8 mm from the weld centre at the advancing and the retreating side of the weld),
- BM.

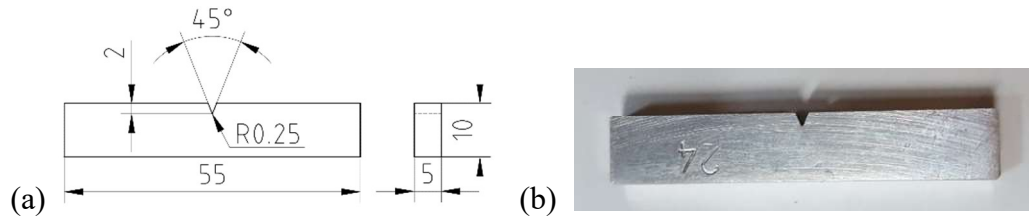


Fig. 8 Geometry of the Charpy specimen and Charpy specimen

**Fracure mechanics tests;** Single edge notch specimens (SENB) were machined from the weld nugget in T-L direction according to ASTM E1820-15a standard. The shape and geometry of the specimen are presented in Figure 9a. Fatigue precrack was done by using Rumul Cractronic machine according to ASTM E1820-15a standard (Figure 10). The SENB specimen with fatigue precrack is shown in Figure 9b. Fatigue precrack was done by R ratio 0.1.

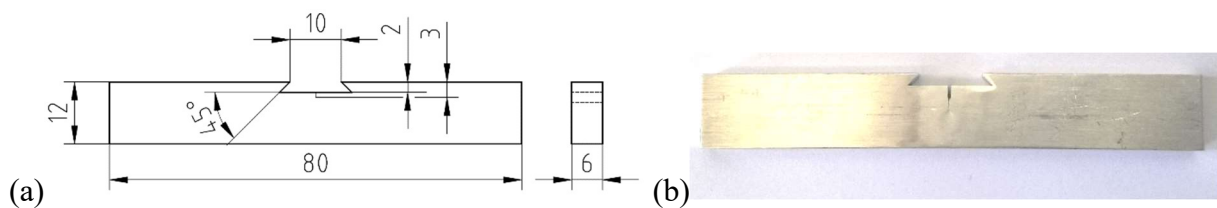


Fig. 9 Geometry of the SENB specimen (a) and SENB specimen with fatigue precrack (b)

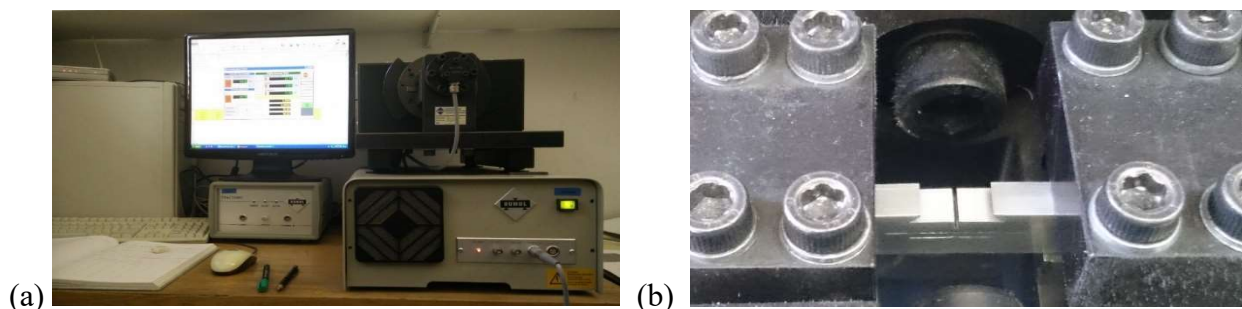


Fig. 10 Fatigue precracking; overall view (a) and detail (b) on Rumul Cractronic machine

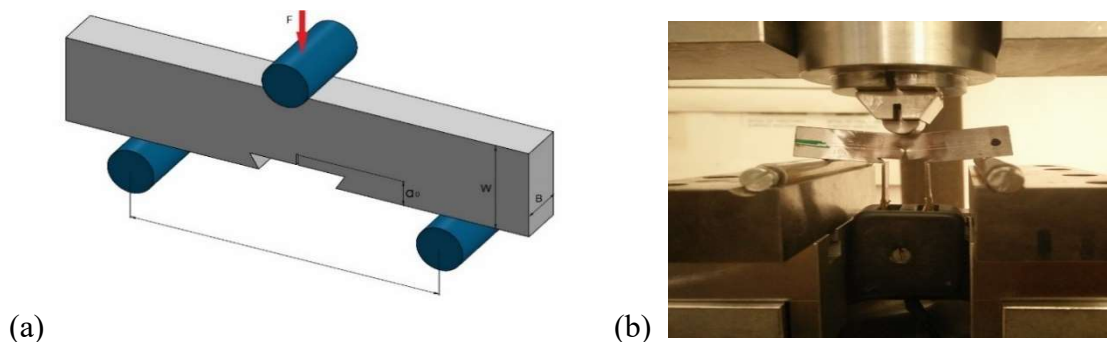


Fig. 11 Testing of the SENB specimen: scheme (a) and detail - Smitweld 1405 machine (b)

Testing and evaluation of the results of the SENB specimens were performed on the SMITWELD 1405 tensile machine unit according to ASTM E1820-15a standards (Figure 11). Marking of the stable crack propagation was carried out by fatigue using  $R$  ratio 0.7 and  $0.5 \times F_{max}$ , where  $F_{max}$  is maximal force obtained at SENB test.

**Hardness measurements:** Macro sections of the weld joint for hardness measurement were machined from both the FSW weld joints. Hardness measurements were performed by Vickers method according to standard EN ISO 9015. Three different directions (lines) of the hardness measurements were carried out. The locations of the directions of the hardness measurements are shown in Figure 12.

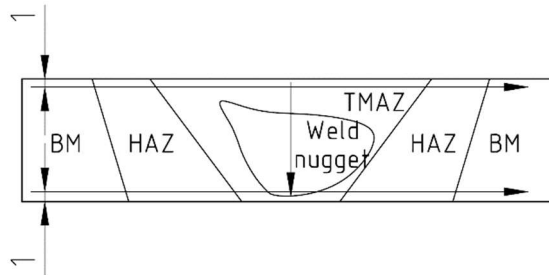


Fig. 12 Locations of the directions of the hardness measurements

**Microstructure analysis:** Micro sections for microstructure analysis were produced from the both FSW joints. Microstructures of the each weld joint were examined under light microscope Nikon Epiphot 300 at different magnifications. Different zones were observed and analysed (weld nugget, TMAZ, HAZ and base material).

#### 4. Results and discussion

Figure 13 represents macrostructures of the macro-sections of the weld joint A and weld joint B. In both photographs it is possible to see:

- asymmetric weld nugget (centre of the figures),
- Thermo Mechanically Affected Zone – TMAZ from advancing and retarding side (near the weld nugget), where a lot of plastic deformations are detected and consequently grains are narrow and stretched,
- Heat Affected Zone – HAZ, which continues TMAZ, is affected by heat without plastic deformation, therefore grains are globular and a little bigger in comparison to base material,
- BMs are possible to see at the far ends of the left or right sides of the both figures.

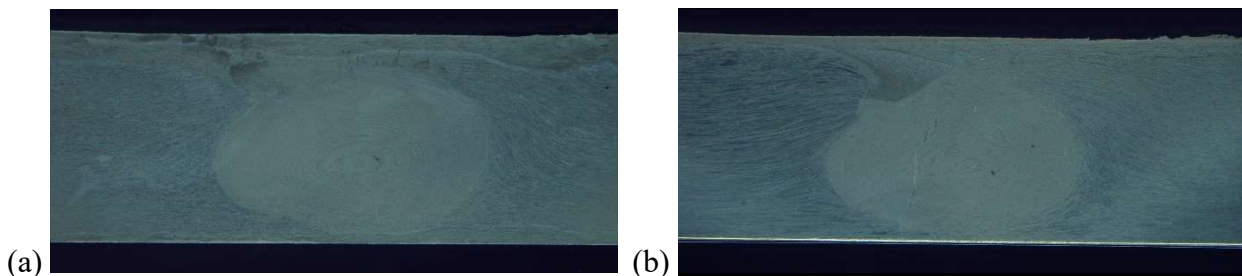


Fig. 13 Macro-section of weld A and B.

Microstructures of the centre of the weld nugget A and the centre of the weld nugget B are shown in Figure 14 and Figure 15 at magnification 50X and at magnification 200X. Materials in weld nugget are heated and mixed due to friction of the tool pin. Obviously it is possible to distinguish different zones in the narrow centre of the both weld nuggets (lighter and darker regions). Both microstructures have fine grains. Some secondary particles are present on grain boundaries (darker spots). Deep investigation of the fractured surface discloses that they are oxide types of inclusions on the base of MgO.

Inclusions are smaller in both weld nuggets in comparison to the BM. Number of the particles are fewer in weld nugget B in than in weld nugget A.

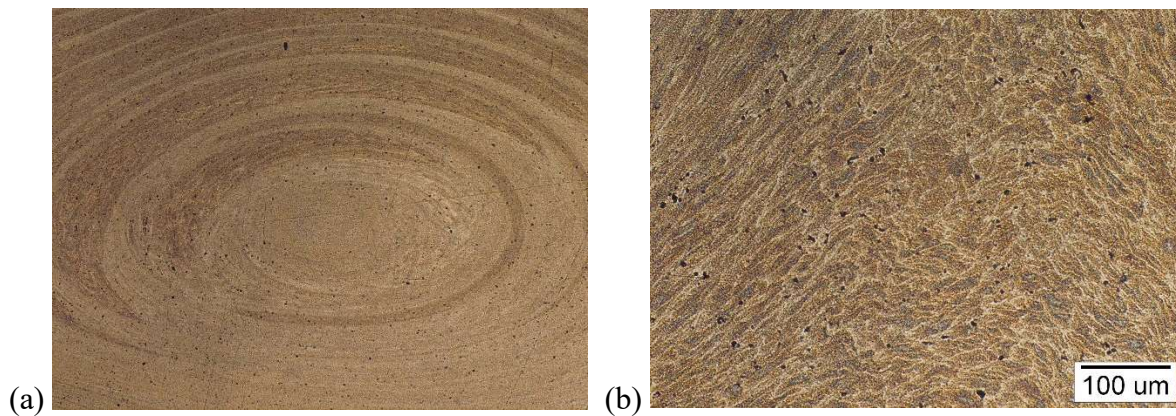


Fig. 14 Microstructure of the weld nugget A - Light microscope, 50X (a), 200X (b)

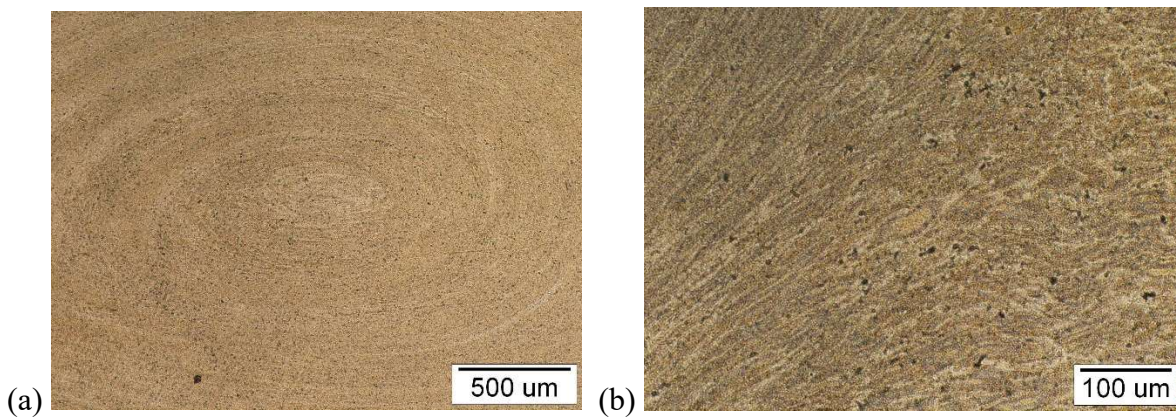


Fig. 15 Microstructure of the weld nugget B - Light microscope, 50X (a), 200X (b)

Results of the tensile tests are shown in Figure 16 and in Table 5. Base material has the highest tensile strength and elongation as well. Tensile strength and elongation of weld joint B is higher than in weld joint A. Both specimens were broken in the region between weld nugget and TMAZ.

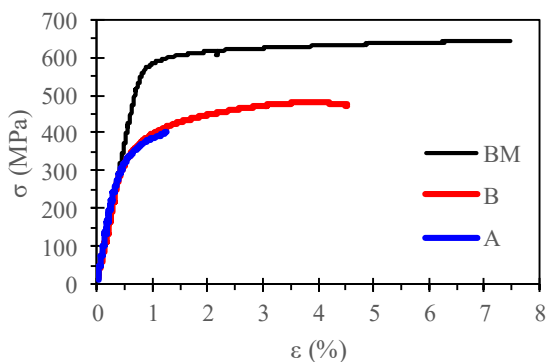


Fig. 16 Results of the tensile testing

Table 5 Results of tensile tests

Material	$R_{p0.2}$ (MPa)	$R_m$ (MPa)	A (%)	E(MPa)
BM	585	643	7.6	74371
A	342	402	0.8	84143
B	360	481	3.9	71363

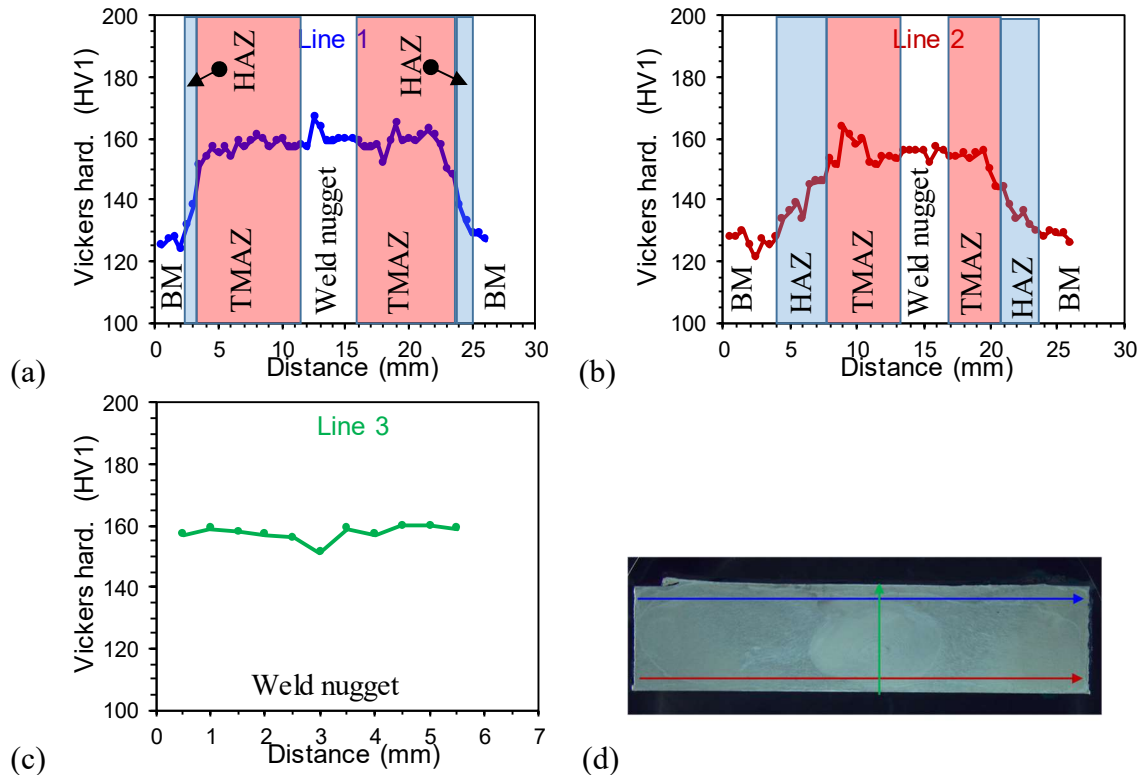


Fig. 17 Results of hardness measurements on weld joint A

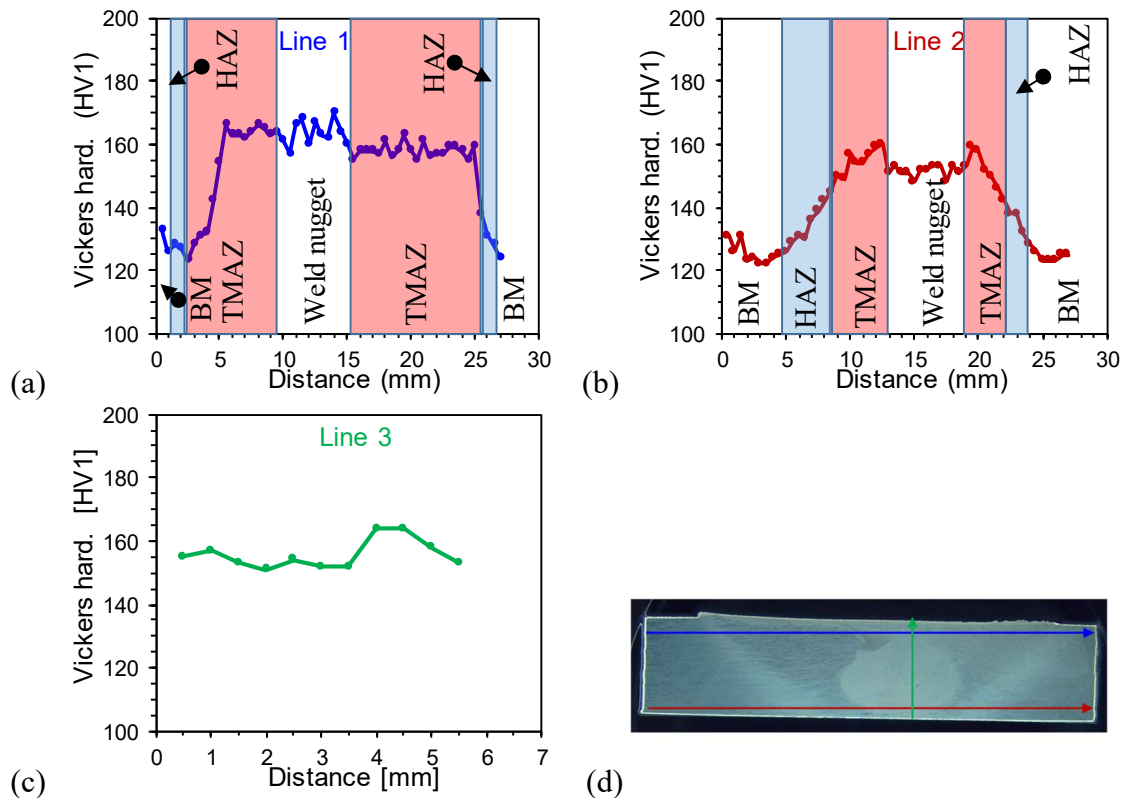


Fig. 18 Results of hardness measurements on weld joint B

Results of the instrumented Charpy impact tests, which had been taken from weld nugget, TMAZ, HAZ and BM, are shown in Figure 16. The Charpy tests were done in the TMAZ and the HAZ regions in the advancing side and in the retarding side of the weld joint. Force versus time ( $F-t$ ) and energy versus time diagrams ( $E-t$ ) were recorded during the instrumented Charpy tests.

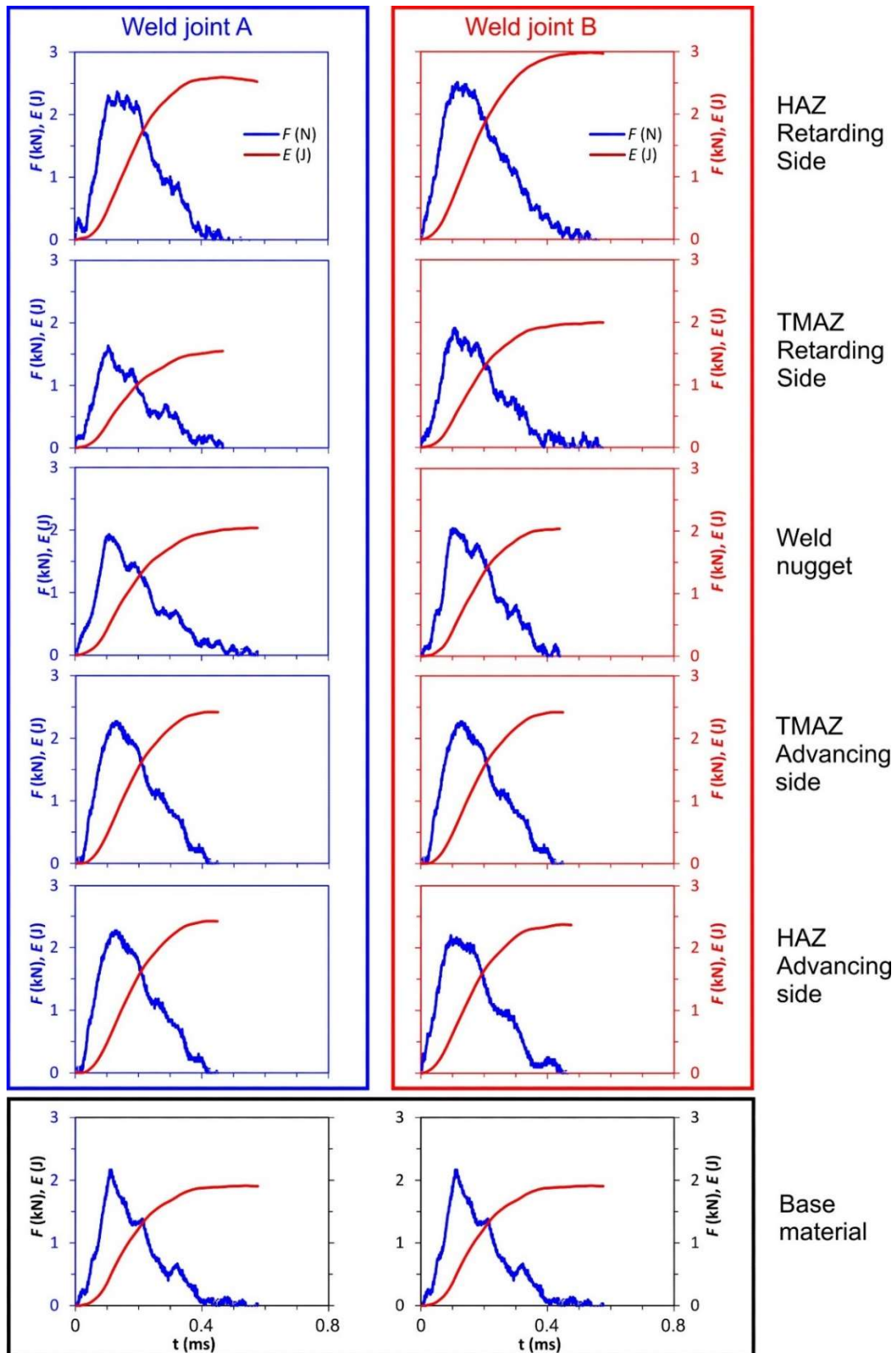


Fig. 19 Results of instrumented Charpy impact tests

After the tests diagrams have been evaluated and total energy has been split into energy for initiation and into energy for propagation of the crack from ISO-V notch stress concentrator. All  $F-t$  and  $E-t$  diagrams are shown in Figure 19. Total energy  $E_t$ , energy for initiation  $E_i$  and energy for propagation  $E_p$  are presented in Figure 20 for all regions of weld joints.

Total energy is very low (less than 3 J) in all regions of both weld joints. Energy for initiation is round  $\frac{1}{4}$  of total energy, and energy for propagation is round  $\frac{3}{4}$  of total energy in all regions of welded joints. The lowest total energy was measured in TMAZ at retarding side in both weld joints.

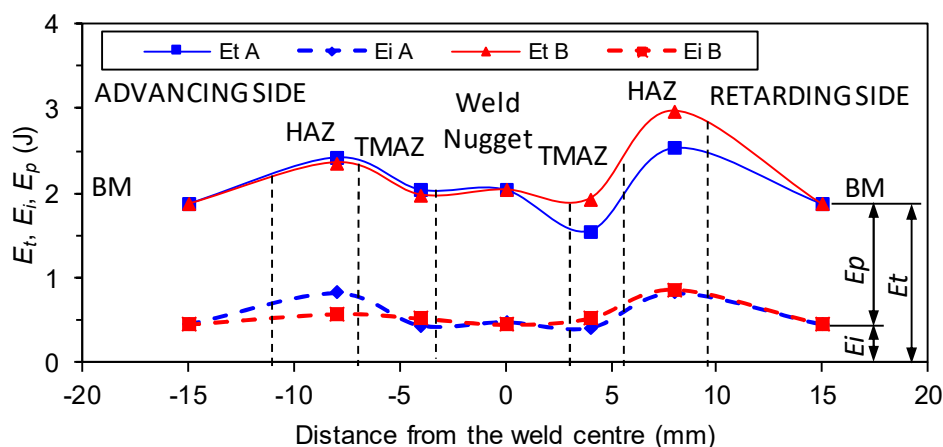


Fig. 20 Energy for initiation and propagation at Charpy impact tests

Fracture mechanics on the SENB specimens in L-T direction from base material and both weld nugget were done according to ASTM E1820-15a standard. Results of the testing are shown in Figure 21, where Force versus Crack Mouth Opening Displacement diagrams (F-CMOD diagrams) are presented.

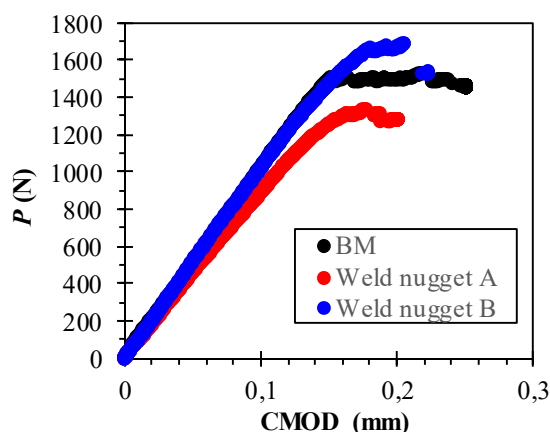


Fig. 21 F-CMOD diagrams for BM, weld nugget A and weld nugget B

J-integral ( $J$ ), crack tip opening displacement ( $\delta$ ) and fracture toughness  $K_{JIC}$  are shown in Table 6. The highest J integral and  $\delta$  was measured in base material. The weld joint B has better J-integral and  $\delta$  than weld joint A. Fracture toughness of the base material and weld material are practically the same, however fracture toughness is higher in weld joint B for 24,7%.

Table 6. Results of SENB tests

Location	$J$ (N/mm or kJ/m <sup>2</sup> )	$\delta$ (mm)	$K_{JIC}$ (MPam <sup>0.5</sup> )
BM	27.67	0.023	28.41
A	12,93	0.019	28.85
B	20.23	0.025	35.42

## 5. Conclusions

Some secondary particles are present on grain boundaries (darker spots). Deep investigation of the fractured surface discloses that they are oxide types of inclusions on the base of MgO. The particles in the weld nugget B are smaller and more uniformly distributed in the weld nugget microstructure in comparison to weld nugget A, what beneficially influences the properties of the weld joint.

Tensile tests demonstrated that the highest weld ultimate tensile strength was obtained in base material (643 MPa). The tensile ultimate strength of the weld joint B (25.2% lower to BM) is higher than weld joint A (37.5% lower to BM). Elongation in BM was 7.6% in comparison to the weld joint B, where 3.9% elongation was measured and the weld joint B where 0.8% elongation was measured.

All values of the energies for fracture of  $6 \times 10$  mm Charpy specimens are low (less than 3 J) for all regions of the weld joints, including the base material. Energy for fracture is higher than in the base material for almost all regions of the weld joints, with exception in TMAZ zone at retarding side, where the lowest energy was measured. Energy for initiation is round 25% of total energy and round 75% of the total energy is energy for propagation in all regions of welded joints.

Results of fracture mechanics testing show that the fracture toughness of the base material is close to weld nugget A (round  $28 \text{ MPam}^{0.5}$ ), however results of the fracture toughness in the weld nugget B are 24.7% higher than in base material (round  $35 \text{ MPam}^{0.5}$ ).

This investigation points out that weld joint B (welded by 80 mm/min) achieves better properties and microstructure than weld joint A (welded by 60 mm/min).

## 6. References

- [1] Bajić, D. (2014): Postupci zavarivanja, Univerzitet Crne Gore, Mašinski Fakultet, Podgorica
- [2] Tušek, J. (2014): Varjenje in sorodne tehnike spajanja materialov v neločljivo zvezo, Fakulteta za strojništvo, Ljubljana, Slovenija.
- [3] Klobčar, D., Kosec L., Pepelnjak, T., Tušek, J. (2012): Microstructure and mechanical properties of friction stir welded almg4.5mn alloy. Engineering Review Vol. 32, No 2.
- [4] <http://www.twi.co.uk/j32/get file/fswmat.html>.
- [5] AWS D17.3/D17 3M 200x An American Nacional Standard, Miami, Florida,2010.
- [6] Projekat proizvodnje legure PD 33, Institut za istrazivanje i razvoj aluminijuma SOUR Kombinat aluminijuma, Titograd, 1986.
- [3] Perović, M. et al. (2012): Friction stir Welding of Strength Aluminijum Alloys and Numerical Simulation of the Plunge Stage. Materials and Technologies, Vol. 46, No. 3.
- [7] Perović, M., Baloš, S., Kozak, D., Bajić, D., Vuherer, T. (2017). Influence of kinematic factors of friction stir welding on the characteristics of welded joints of forged plates made of EN AW 7049 A aluminium alloy, Tehnički vjesnik, Vol 24, No 3.
- [8] Perović, M., Bajić, D., Vuherer, T. (2017): Uticaj broja obrata alata I brzine zavarivanja na mehaničke karakteristike sučeono zavarenog spoja legure Al-Zn-Mg-Cu postupkom trenjem sa miješanjem, Zbornik Dneva verilne tehnike, 2017, Celje, Slovenija, str. 102-107.